# Fast Ion Dynamics in Magnetically Confined Plasma Measured by Collective Thomson Scattering

Henrik BINDSLEV[1)], Stefan K. NIELSEN[1)], Søren B. KORSHOLM[1,2)], Fernando MEO[1)], Poul K. MICHELSEN[1)], Susanne MICHELSEN[1)], Erekle L. TSAKADZE[1)], Paul WOSKOV[2)], Egbert WESTERHOF[3)], J.A. HOEKZEMA[4)], J.W. OOSTERBEEK[4)], Laurie PORTE[5)] and the TEXTOR team

[1)] *EURATOM-Risø National Laboratory, DK-4000 Roskilde, Denmark*
[2)] *MIT Plasma Science and Fusion Center, Cambridge, MA 02139,USA*
[3)] *FOM-Institute for Plasma Physics Rijnhuizen, EURATOM-FOM, The Netherlands*
[4)] *EURATOM-Forschungszentrum Jülich GmbH, Institut für Plasmaphysik, D-52425 Jülich, Germany*
[5)] *CRPP, EURATOM-Confédération Suisse, EPFL, CH-1015 Lausanne, Switzerland*

(Received 3 December 2006 / Accepted 5 June 2007)

Magnetically confined fusion plasmas are mostly heated by small populations of energetic ions. In current devices these fast ions are mainly generated by auxiliary heating, while in ITER fusion generated alpha particles will dominate. A multitude of MHD phenomena, some of them driven by the fast ions, can redistribute or eject the energetic ions prematurely, affecting fusion performance and potentially damaging walls. Theory and modeling of fast ion dynamics in fluctuating or turbulent plasmas is challenging and needs guidance from - and bench marking against - measurements of the fast ion dynamics. Collective Thomson Scattering (CTS) can provide such measurements of the confined fast ions. Here we present CTS measurements of the TEXTOR tokamak plasma which show fast ions responding to sawteeth and display slowdown evolution of the fast ion velocity distribution after switch off of neutral beam heating. The toroidal rotation velocity of the bulk ions is inferred from the measurements. Plans for an ITER fast ion CTS are also briefly discussed.



Keywords: plasma and fusion research, fast and energetic ion diagnostic, collective Thomson scattering, slowdown, rotation velocity

DOI: 10.1585/pfr.2.S1023

## 1. Introduction

Neutral beam injection (NBI) and ion cyclotron resonance heating (ICRH), two of the main heating methods for fusion plasmas, produce small populations of ions with energies well above the average particle energy of the bulk plasma. These fast ions slow down in the plasma because of collisions with the bulk plasma ions and electrons, heating the bulk plasma in the process. In the next generation of fusion experiments, notably ITER, fusion of deuterons and tritons will produce fast alpha particles at such a rate that they become the dominant source of heating of the plasma.

The magnetic topology is generally chosen such that the fast ions remain confined in the plasma in the absence of collisions and perturbations. They follow orbits which drift across magnetic field lines, not only in the gyromotion, but also in the average over many periods of gyration. In their drift orbits the fast ions have several characteristic velocities, including the instantaneous velocity and the toroidal precession velocity for ions undergoing magnetic mirror motion due to the higher field on the inside of the torus. This variety of velocities permit resonant interaction with a multitude of wave phenomena with different phase velocities. Such interaction can shift energy from the ion to the wave or visa versa. At certain points on the ion drift orbits a small change in velocity of the ions can make them change track and follow a drift orbit with a completely different spatial map. If the new orbit intersects a wall, the ion is lost promptly. In any case, the confinement of the fast ion has been affected. The fast ions, having a substantial fraction of the total kinetic energy of the plasma, can also drive waves and turbulence which in turn can affect the confinement of fast ions and bulk plasma.

In ITER on the order of 70 % of the heating will come from fusion alphas. The production of fusion alphas is dependent on the plasma properties which are affected by the fusion alphas. The ITER fusion plasma might thus be quite rich in fast ion related phenomena, and these may be of considerable consequence to the overall fusion performance of ITER. So fast ion populations play an important role in present devices and they will play an even more significant role in the next step devices [1–3]. Of particular interest or concern is the fact that fast ions drive - and are affected by - Alfvén modes [4–9]. Alfvén modes are expected to be particularly prominent in advanced plas-

*author's e-mail: henrik.bindslev@risoe.dk*

mas with reduced central current density (reversed magnetic shear profiles) in which the ion drift orbits are also particularly large and thus more prone to significant redistribution or wave induced transport. Also the ubiquitous sawteeth are affected by fast ions and may redistribute fast ions [10–14].

The interaction of fast ions with the highly non-stationary fusion plasma is complex and rich. To help develop our theoretical understanding of fast ion dynamics and benchmark modeling, it is essential to have experimental observations of the confined fast ion populations resolved in time, space and velocity. In ITER this is particularly important, which is reflected in the ITER diagnostic requirements [15, 16]. The ability of Collective Thomson scattering (CTS) to provide measurements of the fast ion velocity distribution was demonstrated at the Joint European Torus (JET) [17] and the ability of CTS to provide detailed measurements of the temporal evolution of the fast ion velocity distribution under changing conditions was demonstrated at the TEXTOR tokamak [18]. An extensive feasibility study covering millimeter-waves to the Infra red radiation of the $CO_2$-laser, concluded that a CTS with a probe frequency at 60 GHz could meet the ITER diagnostic requirements [19, 20].

CTS is based on the scattering of electromagnetic waves off microscopic fluctuations, principally in the electron distribution, driven by ion motion. In practice a powerful probe beam, for instance in the millimeter-wave range, is sent into the plasma. Microscopic fluctuations in the plasma interact with the incident probe beam and give rise to scattered radiation emanating from all along the probe beam. Part of that radiation is collected by a receiver if the probe and receiver antenna beam patterns overlap. In that case we have a localized measurement of the fluctuations in the *scattering volume* where the probe and receiver beams overlap. They resolve the microscopic fluctuations with wave vector $\boldsymbol{k}^\delta = \boldsymbol{k}^{\mathrm{s}} - \boldsymbol{k}^{\mathrm{i}}$, which provide information on the ion velocity distribution, resolved with respect to the velocity component pointing in the direction of $\boldsymbol{k}^\delta$. Here $\boldsymbol{k}^{\mathrm{s}}$ and $\boldsymbol{k}^{\mathrm{i}}$ are the wave vectors of respectively the received scattered radiation and the probe, both in the scattering volume. Changing the antenna orientations, the location of the scattering volume can be shifted and the resolved $\boldsymbol{k}^\delta$, and hence the resolved velocity direction, can be varied from near parallel to near perpendicular to the magnetic field. A brief introduction to both the theory of CTS and practical considerations are given in ref. [22]. Detailed discussions of the theory can be found in refs. [23–27].

The CTS diagnostic can in principle distinguish different ion specie when the scattering geometry is such that the resolved $\boldsymbol{k}^\delta$ is close to perpendicular to the magnetic field. Distinguishing different ion specie with the same charge to mass ratio does generally require the added assumption that they are in thermal equilibrium. The later is not satisfied by fusion alphas and fast deuterons from NBI. This raised the issue of whether in ITER the CTS signal from fast deuterons from NBI would mask the CTS signal from fusion alphas. This question was addressed in a recent study [21] which concluded that the proposed 60 GHz CTS system for ITER could resolve the fusion alphas against a background NBI fast ion population.

The first CTS measurements of ion temperature in magnetically confined plasmas was done using far infrared radiation [28] using an optically pumped laser as the source of the probing radiation. Using gyrotrons as the source of probing radiation [29] the ion temperature was subsequently measured with millimeter-waves [30, 31]. The first CTS measurement of a fast ion velocity distribution was carried out at JET [17]. Subsequently the temporal evolution of fast ion populations were measured with CTS at TEXTOR [18]. Other CTS experiments at TFTR [32], JT60-U [33] and FTU [34], though not yielding ion data, contributed by widening the experience with operating CTS diagnostics.

The breakthrough with routine CTS measurements of fast ion populations in magnetically confined plasma, resolving on the order of 100 time slices at intervals of 4 ms in each plasma shot, was achieved with the millimeter-wave CTS at TEXTOR [18]. We will discuss some of these results here. Part of the present discussion will follow closely part of that of [18], expanding on some elements. In section 2 we describe the experimental setup. Raw CTS data and extraction of CTS data are discussed in section 3. In section 4 the measured fast ion evolution at sawteeth and the slowdown after switch off of auxiliary heating are presented. Plans for ITER are briefly discussed in section 5 and conclusions are given in section 6.

## 2. The TEXTOR CTS System

The probing radiation for the TEXTOR CTS is provided by a 110 GHz gyrotron operated at 150 kW. With a central toroidal field of 2.6 tesla the CTS spectra are at a local minimum in the electron cyclotron emission (ECE) spectrum between the fundamental and second harmonic ECE features. The probing radiation is launched from the low field side in the equatorial plane and the receiver antenna is located about 20 cm above the entry of the probing beam. Both transmitter and receiver have steerable, near Gaussian beam, antenna patterns. The receiver antenna is shown in figure 1.

Outside the vessel the received radiation is transmitted to the detector by a quasi optical transmission line which includes a universal polarizer consisting of two rotatable grooved mirrors to select scattered radiation with a given elliptical polarization and hence select radiation in one of the plasma normal modes of propagation (ordinary or extraordinary mode). The probing radiation is transmitted from the gyrotron via a quasi optical transmission line which also includes a universal polarizer permitting the probe radiation to be coupled to a normal mode. Generally O-mode is used for both probe and receiver. The steering

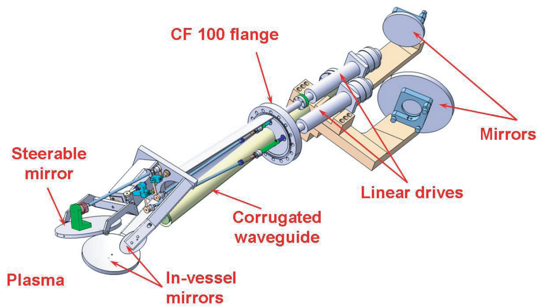


(a) Drawing of CTS receiver antenna

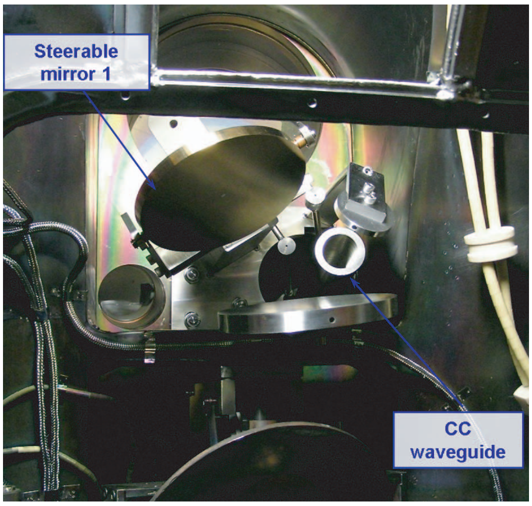


(b) Photo of CTS receiver antenna

Fig. 1 Drawing and picture of the upgraded CTS antenna. The picture is taken from inside the TEXTOR vessel. Inside the vacuum the antenna consists of a flat steerable mirror, two curved mirrors and a circular corrugated waveguide for transmitting the received radiation out through the narrow port. The drawing also shows two external mirrors which are part of the quasi optical transmission line to the receiver.

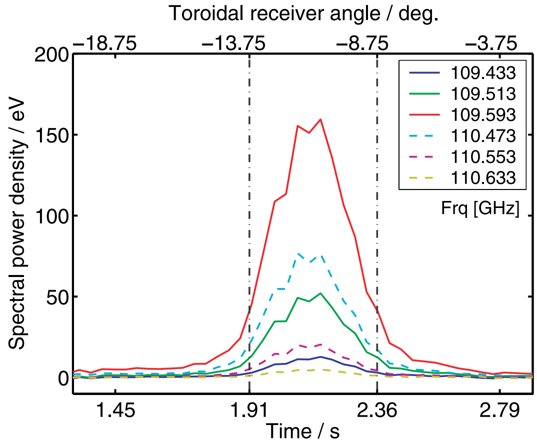


Fig. 2 (Figure 1 in [18]) CTS spectral data recorded for an ohmic plasma where the toroidal angle $\phi_r$ of the receiver viewing direction was scanned during the plasma shot. The plot shows CTS spectral power density in a number of channels vs. time and $\phi_r$. Receiver and probe beams go through overlap for a variation of 5° of $\phi_r$. With a distance from receiver antenna to scattering volume of 50 cm this corresponds to a width of the scattering volume of 4 cm in the direction perpendicular to the probe and receiver beam directions (perpendicular to $\boldsymbol{k}^{\mathrm{i}}$ and $\boldsymbol{k}^{\mathrm{s}}$). In the direction of $\boldsymbol{k}^{\delta}$ the extent of the scattering volume is approximately 5/2 times larger. Shot number 100467. $\angle(\boldsymbol{k}^{\delta}, \boldsymbol{B}) = 110$. Scattering volume at $R = 1.8\,\mathrm{m}$, $z = 0\,\mathrm{m}$.

ranges for the probe and receiver beams permit the location of the scattering volume to be shifted across most of the plasma cross section and they permit the resolved velocity direction to be varied from near parallel to near perpendicular to the magnetic field. The radial resolution is approximately 5 cm when the scattering geometry is such that the velocity directions near parallel to the magnetic field are resolved and approximately 10 cm when near perpendicular directions are resolved. This is corroborated by the data displayed in figure 2 which show the spectral power densities recorded in a number of channels while the toroidal viewing angle of the receiver was scanned during a plasma shot. These data are also good evidence that the signals are indeed the result of scattering from the probe beam in the plasma.

The received scattered radiation is detected using a hetrodyne receiver with 32 (upgraded to 42) spectral channels with bandwidths from 80 MHz to 750 MHz, giving complete coverage from 107 GHz to 113 GHz. Notch filters are used to reduce stray radiation. The diagnostic is calibrated using thermal emission from the empty vacuum vessel and ECE. Further details on the diagnostic and its upgrades can be found in references [35–39].

A 50-channel CTS diagnostic, similar to the TEXTOR CTS, has been installed on the ASDEX Upgrade tokamak. The source of the probe radiation will be the 105 GHz frequency mode of operation of a new gyrotron with powers up to 800 kW for 10 s. AUG has recently been equipped with four new electron cyclotron resonance heating (ECRH) systems. For CTS the probing radiation is delivered to the plasma using one of the ECRH systems as the probe. Another ECRH line (steerable antenna, transmission line and universal polarizer) is used in reverse as part of the CTS receiver. For CTS operation the scatterede radiation traveling in reverse in the ECRH transmission line is intercepted by a movable mirror to direct it to the receiver.

## 3. Data Analysis

The spectral power density of the CTS signals in the frequency ranges carrying fast ion information is typically around 1-10 eV. The spectral power density of ECE and detector noise is typically 10-100 eV, implying a raw signal to noise ratio of 0.01 to 1. For convenience we will refer to ECE plus detector noise as ECE. To distinguish the fast ion CTS signal with spectral power density around 1-10 eV from the ECE background we modulate the gyrotron with a

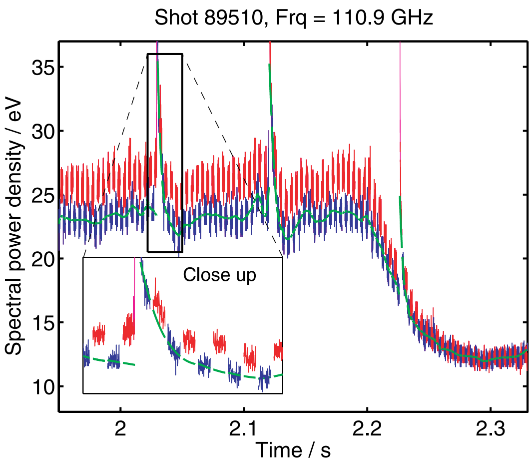


Fig. 3 (Figure 2 in [18]) Raw data time trace for a CTS channel. Blue indicates ECE background and red refers to gyrotron on-time (CTS + background). The green line represents the reconstructed background during the gyrotron probing time.

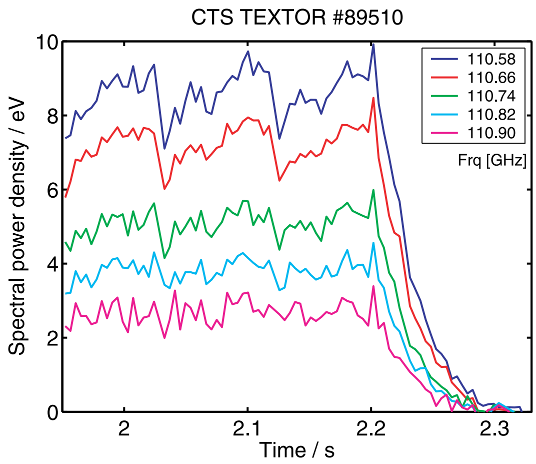


Fig. 4 (Figure 3 in [18]) Time traces of the CTS spectral power densities in five channels. The channels are labeled by their center frequencies. Uncertainty approximately 0.4 eV. This process is due to the stochastic process of scattering, variations in the gyrotron pulse power, variations in overlap and the ECE subtraction procedure. The latter contributes less than 0.1 eV to the uncertainty. Shot number 89510.

period of 4 ms and a 50 % duty cycle, giving a time resolution of 4 ms. Figure 3 shows the calibrated data recording for the spectral power density in the channel centered at 110.9 GHz plotted versus time for shot 89510. The samples recorded when the gyrotron was off (on) are shown as blue (red) and are thus due to ECE (ECE + CTS). ECE signals are recorded when the gyrotron is off and continuously monitored in channels several GHz away from the gyrotron frequency where no scattered radiation is observed nor expected. From these signals the ECE during gyrotron pulses can be estimated for each channel. The green line in figure 3 shows such an ECE estimate. The CTS signal is estimated by subtracting the ECE estimate from the signals recorded when the gyrotron is firing. At the chosen magnetic field very little of the probe radiation from the gyrotron is absorbed by the plasma and the ECE is thus not perturbed significantly by the probe radiation. The accuracy and robustness of this procedure is verified by the zero average estimate of the CTS signal in (a) the frequency ranges beyond that of the expected CTS spectrum, and (b) for the full spectrum when there is no overlap between the probe beam and the receiver beam. From these data we can also estimate that the ECE subtraction procedure generates an uncertainty of less than 0.1 eV in the estimated CTS signal integrated over one gyrotron pulse. In the event that the ECE is poorly fitted, for instance near in a sawtooth crash, then the CTS data are automatically discarded. This very rarely happens though. The quality of the ECE fit is automatically tested as part of the data validation.

The ECE entering the receiver in the frequency bands of interest for CTS is emitted from the plasma edge and hence outside the sawtooth inversion radius. The sawteeth thus give rise to sudden rises in the ECE spectral power density in the frequency band where the CTS signal is as seen in figure 3 where sawteeth occur at at 2.03, 2.12 and 2.23 seconds. Despite the resulting strong perturbations in the background, against which the CTS signals are to be extracted, the estimated CTS signal at 110.9 GHz has no visible signature of sawteeth as seen in figure 4. Here the CTS time trace for 110.9 GHz is plotted together with CTS signals at four other frequencies for shot 89510. In the channels covering the frequencies from 100.58 GHz to 100.74 GHz clear signatures of sawteeth are present, which we ascribe entirely to sawtooth related variations in the CTS spectral power density. We do this on account of the robustness of the ECE subtraction and because the ECE variation in all the CTS channels are very similar. This is clearly brought out in plots of the raw data and can be understood from the fact that the relative frequency variation from centre to edge of the CTS spectrum is approximately 1 % corresponding to a 1 cm shift of the EC resonance on the high field side of the plasma which has a minor radius of 50 cm. This implies that for all CTS channels the ECE emission comes from the scrape off layer and is far removed from the inversion radius where the ECE time traces vary substantially as a function of frequency.

In figure 5 the CTS spectral power density for shot 89510 is plotted as a function of time and frequency over the full CTS bandwidth with data from the 21 channels from which data were recorded. No data are shown for frequencies near the probe frequency where the notch filter blocks signals.

From the CTS spectral power density, the fast ion 1D velocity distribution is inferred by means of a least squares fitting procedure (LSN) [40] which provides the estimate corresponding to the maximum of the *posterior*; that is the

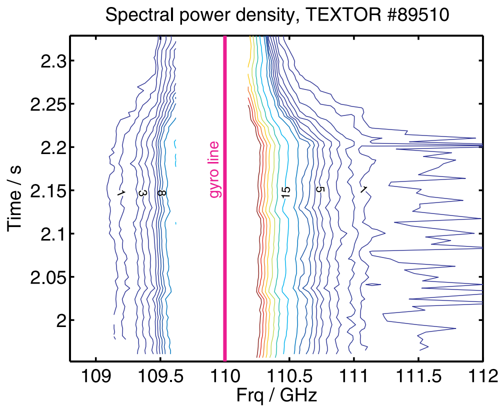


Fig. 5 (Figure 4 in [18]) CTS spectral power density as a function of time and frequency. The central part of the spectrum is blocked by a notch filter. Shot number 89510.

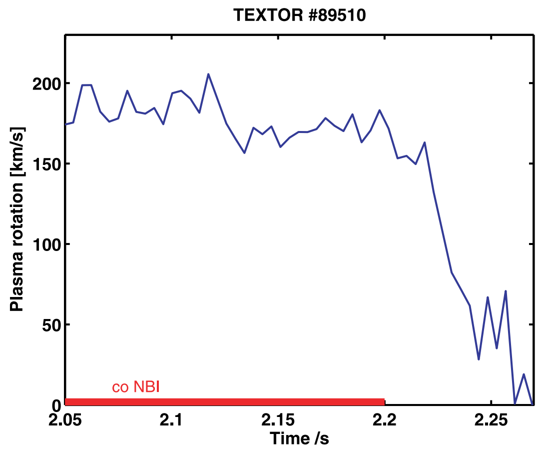


Fig. 6 Toroidal rotation velocity of thermal ion population vs. time inferred from wings of thermal ion CTS spectral feature. Auxiliary heating is on till 2.2 seconds.

most probable values of the parameters characterizing the ion velocity distribution and a few other parameters of interest. The posterior and hence LSN integrates the information from the CTS measurements with *prior* (i.e. other) information with finite uncertainty, e.g. information from other diagnostics, providing the optimal inference taking all information, and notably also all uncertainties, into account. LSN also accommodates a large number of *nuisance parameters*, parameters which the forward model (the model of the CTS spectrum) depends on but which we are not seeking to estimate. Nuisance parameters include the scattering angle or the electron temperature. The forward model used in the inference is a fully electromagnetic model of CTS with magnetized thermal ions [26]. The inferred distribution is shown in various forms in figures 6, 7, 8 and 9.

In the inference on the ion velocity distribution we assume that it consists of a thermal part and a super-thermal part. For the thermal part we assume that the velocity distributions are Maxwellian, characterized by a common temperature for bulk ions and impurity ions and by the respective densities of bulk ions and impurity ions. The notch filter blocks a significant part of the feature in the CTS spectrum containing information on the thermal ions. From what is present of the thermal ion feature in the recorded CTS spectra and including information on impurity ion densities from other diagnostics, it is, nonetheless, possible to estimate the thermal ion temperature, and the thermal ion toroidal drift velocity. The latter is plotted in figure 6. The assumption about the ion velocity distributions being thermal at lower velocities is the reason why the plot in figure 8 shows the ion velocity distribution also at low velocities, for which inference could not have been made without this assumption. That the distribution is thermal at these low velocities is supported by our Fokker-Planck simulations with NBI heating.

With the recent upgrade of the TEXTOR CTS more detail of the thermal feature can be recorded and the inference on thermal ion properties, including the toroidal rotation velocity, thus become more accurate and reliable.

For the super-thermal part of the velocity distribution the functional form of the model function used in the inference is essentially a trapezoidal function, that is a curve consisting of straight line segments connecting a finite set of points which we refer to as nodes. The trapezoidal function is rounded for numerical convenance at the nodes to eliminate discontinuities in the gradient of the function. The function is thus defined by the coordinates of the nodes. The number of nodes and the abscissae (that is the velocity values) of the nodes define a particular type of trapezoidal function. Having selected the number of nodes and their abscissae, the trapezoidal function is defined by the ordinates, that is the phase space densities, of each node. These are the parameters which define our super-thermal velocity distribution and which are among the parameters of interest estimated by the LSN fit. In the inference we select the number of nodes and their abscissae on the basis of how much fast ion information is in the CTS spectra. The number of degrees of freedom, corresponding to the number of nodes, is below, but can be close to, the number of channels covering the super-thermal ion feature in the CTS spectra. The ion velocity distribution plotted in figures 6 7, 8 and 9 are the sum of the drifting Maxwellian for the bulk and the trapezoidal function for the super-thermal part.

## 4. Discussion of Data

In TEXTOR shot 89510 the fast ions were generated by ~1.3 MW neutral beam injection of ~50 keV deuterons in the co-current direction and by ~1.0 MW minority ion cyclotron resonance heating (ICRH) of hydrogen with a frequency of 38 MHz giving rise to a resonance layer slightly on the low field side of the vessel center. The orientations of the probe and receiver beams were such that

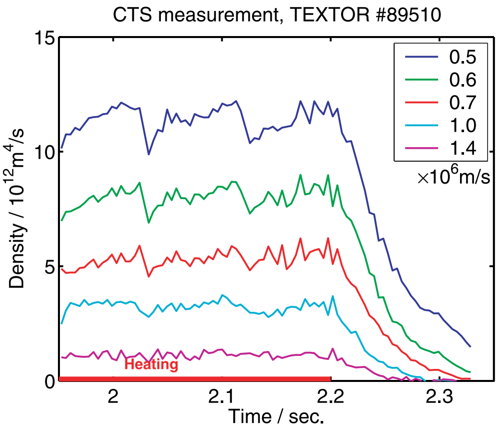


Fig. 7 (Figure 5 in [18]) Ion phase space density vs. time at a number of velocities. Auxiliary heating is on till 2.2 seconds. Sawteeth are in evidence at lower velocities but not at higher.

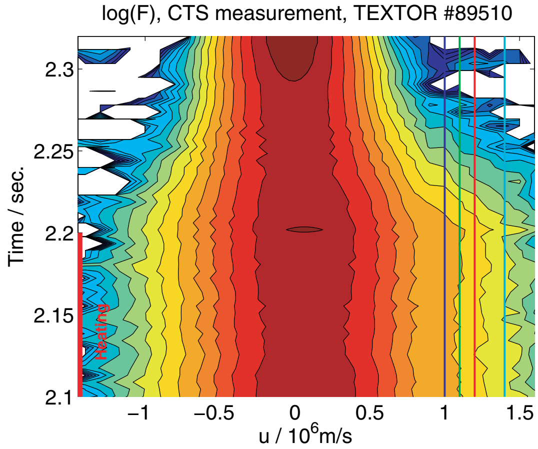


Fig. 8 (Figure 6 in [18]) Contour plot of the logarithm of the measured ion velocity distribution. The auxiliary heating was turned off at $t = 2.2$ sec. Time traces are shown in figure 9 for the velocities indicated in this figure with vertical lines.

the resolved fluctuation wave vector, $\boldsymbol{k}^{\delta}$, and hence the direction in which the velocity was resolved, made an angle to the static magnetic field of 113°. The scattering volume was at $R = 1.61 \pm 0.08$ m and $z = 0 \pm 0.03$ m. These values were estimated by ray tracing. The scattering volume was located on the high field side of the plasma center, close to the tangent radius of the neutral beam injector. The majority of the beam ions present in the scattering volume are thus ionized with a velocity close to parallel to the static magnetic field. The spatial distribution of ICRH heated fast ions is generally predicted to fall off very rapidly on the high field side of the ICRH resonance layer [41, 42]. This suggests that the fast ions in the scattering volume in shot 89510 are mainly beam ions. Sawteeth are in clear evidence in the ion velocity distribution measured in shot 89510 during the NBI flattop for velocities in the range 0.5 to $0.9 \times 10^6$ m/s, but not at higher velocities. This result is reproducible for shots with the measurement on the high field side and velocities resolved in a direction near perpendicular to the magnetic field. In other shots, where either the measurement was on the low field side and near perpendicular velocities resolved, or the resolved direction was near parallel to the magnetic field and the measuring volume close to the vessel center, there was no evidence of sawtooth activity in the ion velocity distribution. This despite the presence of sawteeth with the same magnitude and period as in shot 89510.

The auxiliary heating was turned off at $t = 2.2$ sec after which the fast non-Maxwellian part of the velocity distribution slows down and thermalizes. The measured relaxation of the fast ion velocity distribution, shown in figures 8 and 9, is in remarkable agreement with the results of Fokker-Planck modelling results [18].

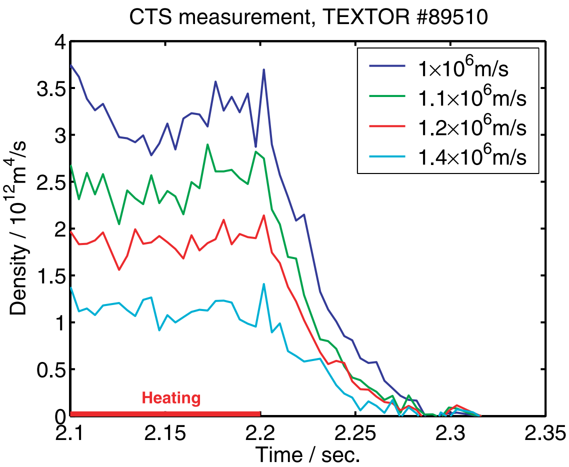


Fig. 9 (Figure 8a in [18]) Time traces of the ion phase space density at a number of velocities.

## 5. ITER CTS

The current CTS experiments are the stepping stone for a CTS system on ITER to measure fast fusion alphas in a burning plasma. A comprehensive feasibility study was carried out [19] to identify the CTS design, including choice of probe frequency, which would satisfy ITER measurement requirements for confined fusion alphas. The study concluded that a dual forward and back scattering system with a probe frequency around 60 GHz is the only CTS system that satisfies all criteria with present or near term technologies. A summary of the feasibility and conceptual design study can be found in references [20] and [44]. The proposed design was optimized to satisfy requirements on accuracy and detail of the inferred fast ion velocity distribution (which can be summed up in the *resolving power* [43]), spatial resolution, time resolution and robustness over a broad range of plasma parameters.

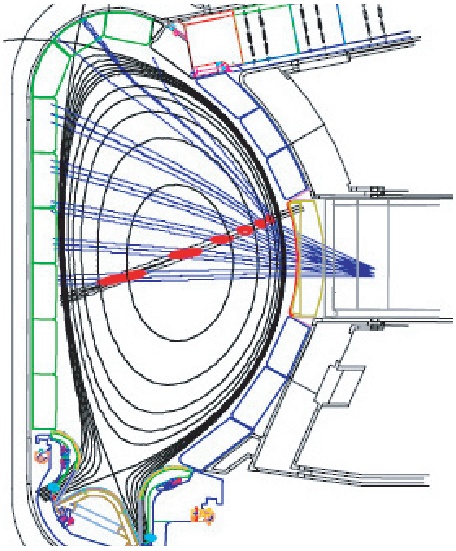

Fig. 10 Beam traces for the low field side-back scattering CTS for ITER. Scattering volumes shown in read.

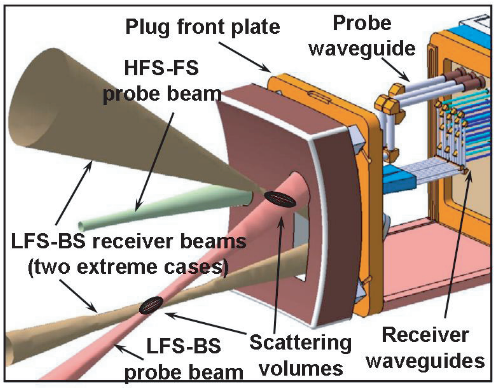


Fig. 11 The CTS design in port plug # 12 with the 3D Gaussian beams. The two extreme LFS-BS receiver beams are in brown, the LFS-BS probe beam is shown in pink, and the HFS-FS probe beam in light green. The black ellipses are the scattering volumes at the two spatial limits of the measurement.

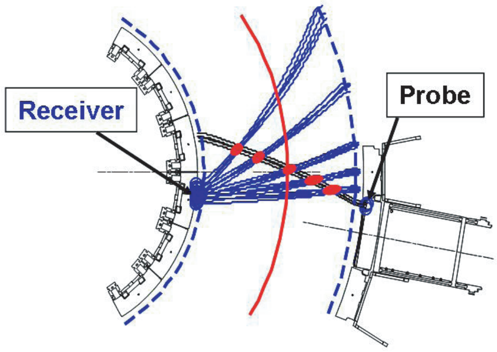


(a) Top view of beam traces

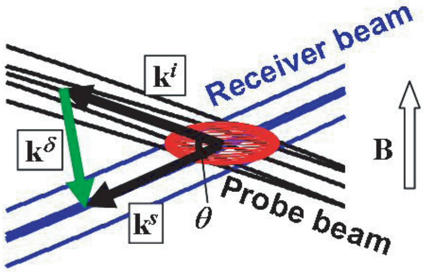


(b) Zoom on one scattering volume

Fig. 12 Probe and receiver beams of the ITER CTS with high field side receivers. (a) Top view of beam traces for the HFS-FS with a LFS probe launcher and HFS-FS detector. (b) Zoom in on one of the scattering volumes (in red). Shown are the wave vectors of the received scattered radiation $\boldsymbol{k}^s$, the incident probe radiation $\boldsymbol{k}^i$, and the fluctuation vector $\boldsymbol{k}^\delta = \boldsymbol{k}^s - \boldsymbol{k}^i$ which is near parallel to the magnetic field $\boldsymbol{B}$.

The 60 GHz frequency chosen in the ITER CTS system is a compromised between low ECE levels (favoring low frequencies) and acceptable refraction (favoring high frequencies) for a wide range of operating scenarios envisioned for ITER. The system is capable of measuring the fast ion velocity distribution parallel and perpendicular to the magnetic field at 10 different radial locations simultaneously. The design is robust technologically, with no moveable components near the plasma. The fast ion CTS diagnostic consists of two separate systems. Each system has its own probe launched from the low field side and separate set of detectors on respectively the low field side (LFS) and the high field side (HFS). The Low Field Side - Back Scattering (LFS-BS) system system, shown in figures 10 and 11, measures the fast ion distribution resolved with respect to the component of the ion velocity which is near perpendicular to the magnetic field. It consists of near radially directed probe and receiver antennae, both located in the equatorial port #12. The High Field Side - Forward Scattering (HFS-FS) part of the CTS diagnostic, illustrated in figures 12 and 13, measures the fast ion distribution resolved with respect to the ion velocity component near parallel to the magnetic field. It consists of a probe launcher located in the mid-plane port #12 and a receiver, mounted on the inner vacuum vessel wall, that views the plasma from between two blanket modules.

The HFS-FS comprises a set of quasi-optical mirrors mounted on the vacuum vessel wall viewing the plasma through the gap between the blanket modules. In order to ensure enough CTS signal to satisfy the ITER measurement requirements [19], a blanket cut-out is required creating an effective vertical height of the slot of 30 mm. The radiation is collected and coupled to an array of horns. The earth strap mounting block, used for electrically grounding the blankets, limits the distance between the mirror and the horn array. The vertical distance available is 303 mm. The limited space available necessitates a multi mirror beam conditioning system for coupling the received radiation into wave guides via horns. The first mirror, in direct view

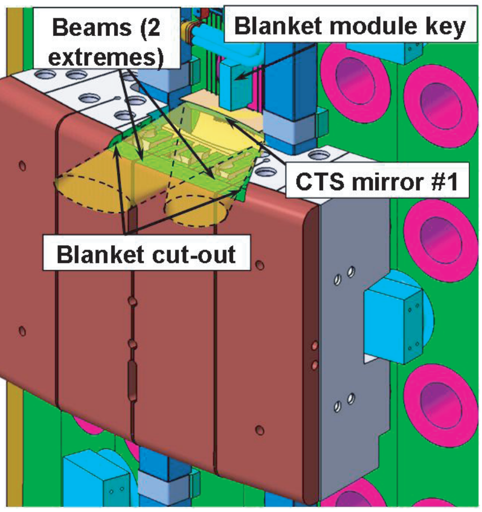


Fig. 13 The CTS HFS-FS receiver viewed from the plasma. The blanket #4 is not shown.

of the plasma, is cooled by the vacuum vessel wall through conduction. Each horn collects scattered radiation from a different location in the plasma. This radiation is transmitted upward along the vessel wall via fundamental wave guides, behind the first mirror, connecting to tapers that are couple to overmoded waveguides. The transmission line consists of 2 sets of five overmoded waveguides that reside along the vacuum vessel wall.

## 6. Conclusions

In conclusion, current fast ion CTS experiments at TEXTOR demonstrate the ability of CTS to provide detailed information on the dynamics of confined fast ions. The evolution of the ion velocity distribution in connection with sawteeth was measured and notable dependencies on velocity, resolved velocity direction and spatial location were apparent. The relaxation of the ion velocity distribution after switch off of auxiliary heating could be resolved. These results represent a breakthrough for the use of millimeter-wave collective Thomson scattering for diagnosing confined fast ions in fusion plasmas, and is an important milestone in preparing this diagnostic method for use at ITER.


[1] W.W. Heidbrink and G. Sadler, Nucl. Fusion **34**, 535 (1994).
[2] J. Jacquinot *et al.*, Nucl. Fusion **39**, 2471 (1999).
[3] S.D. Pinches*et al.*, Plasma Phys. Controlled Fusion **46**, B187 (2004).
[4] M. Rosenbluth and P.H. Rutherford, Phys. Rev. Lett. **34**, 1428 (1975).
[5] C. Cheng and M. Chance, Phys. Fluids **29**, 3695 (1986).
[6] V.S. Belikov, Y.I. Kolesnichenko and V.V. Lutsenko, Nucl. Fusion **35**, 207 (1995).
[7] W. Kerner *et al.*, Nucl. Fusion **38**, 1315 (1998).
[8] K. Wong, Plasma Phys. Controlled Fusion **41**, R1 (1999).
[9] M. Ishikawa *et al.*, Nuclear Fusion **45**, 1474 (2005).
[10] D.J. Campbell *et al.*, Phys. Rev. Lett. **60**, 2148 (1988).
[11] J. Graves *et al.*, Plasma Phys. Controlled Fusion **47**, B121 (2005).
[12] Y. Kolesnichenko *et al.*, Nucl. Fusion **40**, 1325 (2000).
[13] H. Duong and W. Heidbrink, Nucl. Fusion **33**, 211 (1993).
[14] F.B. Marcus *et al.*, Nucl. Fusion **34**, 687 (1994).
[15] Iter final design report, design requirements and guidelines level 1 (drg1), report no. g a0 gdrd 2 01-07-13 r 1.0 (2001).
[16] V. Mukhhovatov *et al.*, *Diagnostics for Experimental Thermonuclear Fusion Reactors 2* (Plenum, New York 1998), chap.2, p.25.
[17] H. Bindslev *et al.*, Phys. Rev. Lett. **83**, 3206 (1999).
[18] H. Bindslev *et al.*, Phys. Rev. Lett. **97**, 205005 (2006).
[19] H. Bindslev, F. Meo and S.B. Korsholm, *Iter fast ion collective thomson scattering-feasibility study, report, efda contract 01.654* (2003), available at www.risoe.dk/fusion/cts/iter.
[20] H. Bindslev *et al.*, Rev. Sci. Instrum. **75**, 3598 (2004).
[21] J. Egedal *et al.*, Nucl. Fusion **45**, 191 (2005).
[22] H. Bindslev, J. Plasma and Fusion Research **76**, 878 (2000).
[23] A. Sitenko and Y. Kirochkin, Sov. Phys. Usp. **9**, 430 (1966).
[24] R. Aamodt and D. Russel, Nucl. Fusion **32**, 745 (1992).
[25] H. Bindslev, Plasma Phys. Controlled Fusion **35**, 1615 (1993).
[26] H. Bindslev, J. Atmos. Terr. Phys. **58**, 983 (1996).
[27] H. Bindslev *Strong microwaves in plasmas* (Russian Academy of Sciences, Institute of Applied Physics, Nizhny Novgorod 1996), vol.1, p.109.
[28] R. Behn *et al.*, Phys. Rev. Lett. **62**, 2833 (1989).
[29] P. Woskoboinikow, D.R. Cohn and R.J. Temkin, Int. J. Infrared and Millimeter Waves **4**, 205 (1983).
[30] E. Suvorov *et al.*, Plasma Phys. Controlled Fusion **37**, 1207 (1995).
[31] J. Hoekzema *et al.*, Rev. Sci. Instrum. **68**, 275 (1997).
[32] J. Machuzak *et al.*, Rev. Sci. Instrum. **68**, 458 (1997).
[33] T. Kondoh *et al.*, Rev. Sci. Instrum. **72**, 1143 (2001).
[34] U. Tartari *et al.*, Nucl. Fusion **46**, 928 (2006).
[35] H. Bindslev *et al.*, in *Proc. 26th EPS Conf. on Contr. Fusion and Plasma Physics, Maastricht, 14-18 June 1999*, ed. R. Pick, Paris, vol.23J, p.765.
[36] H. Bindslev *et al.*, Fusion Engineering and Design **53**, 105 (2001).
[37] L. Porte *et al.*, Rev. Sci. Instrum. **72**, 1148 (2001).
[38] S. Michelsen *et al.*, Rev. Sci. Instrum. **75**, 3634 (2004).
[39] S. Korsholm *et al.*, Rev. Sci. Instrum. **77**, 10E514 (2006).
[40] H. Bindslev, Rev. Sci. Instrum. **70**, 1093 (1999).
[41] T. Hellsten *et al.*, Nucl. Fusion **44**, 892 (2004).
[42] V. Kiptily *et al.*, Nucl. Fusion **42**, 999 (2002).
[43] H. Bindslev, *Proc. 8th Int. Symp. Laser Aided Plasma Diagnostics, Doorwert, NL, 22-26 Sept. 1997, ed. Tony Donne, FOM, NL*, p.265. Also available at www.risoe.dk/fusion/CTS/publications/pdf/LAPD8.pdf
[44] F. Meo *et al.*, Rev. Sci. Instrum. **75**, 3585 (2004).